IEEE Robotics and Automation Letters (RA-L) paper, presented at ICRA 2026, Vienna, Austria. Cite as RA-L paper.

Design and Control of Isoperimetric Robot from Tape Springs

Jackson Hancey[1], Fisk Lundgreen[1], and Nathan Usevitch[1]

***Abstract*—Isoperimetric robots can dramatically change shape to adapt to different tasks. They are built from triangle modules, each formed by a continuous structural member that passes through three roller units, one at each corner. The robot changes shape as the roller units drive along the structural member, changing the location of the joints. Previous designs used inflated fabric tubes as the structural member, but these systems are prone to leaking and changes in pressure due to temperature effects. We present an isoperimetric robot composed of tape-springs (curved spring steel tapes) as the primary structural member, and assemble an octahedron robot. We detail the design of the roller modules that can drive along the tape spring. We also show that with tape springs, all three roller units at the vertices of each triangle can drive along the tape spring. This increases the robot's speed moving between configurations and enables new types of behaviors, such as motion of the beam without motion of the rollers. We also present an optimization procedure for the tape spring isoperimetric robot that minimizes the time required to reach a desired configuration, assuming each roller is limited to a maximum speed.**

***Index Terms*—Compliant Joints and Mechanisms, Cellular and Modular Robots, Parallel Robots**

I. Introduction

Modular robots offer versatile and adaptable solutions for dynamic environments by enabling self-reconfiguration and robust movement. Among these, isoperimetric truss robots, composed of interconnected triangular units, are particularly effective due to their structural stability and ability to change shape. Previous isoperimetric robots, such as the one presented in [1], used inflatable tubes as structural members to achieve a small compact size when deflated and to be inherently human-safe. Inflatable isoperimetric robots have been considered as a potential modular robot for lunar or space applications [2], but possible air leaks or large changes in internal pressure with temperature present significant obstacles. To address these challenges, we propose an isoperimetric robot in which the primary structural members are tape springs (curved spring steel tapes).

Our robot, shown in Fig. 1, consists of folded tape springs, rollers, and spherical joints that form triangular units. Each triangle is made up of a continuous structural member (two tape springs attached back-to-back) that passes through three roller units, one at each corner. Each of these roller units is then connected via spherical joints to create a reconfigurable truss structure. Actuation is achieved by driving the motorized roller units along the length of the tape spring. Moving each roller shortens one edge of the triangle and lengthens another while preserving the overall perimeter of the triangle.

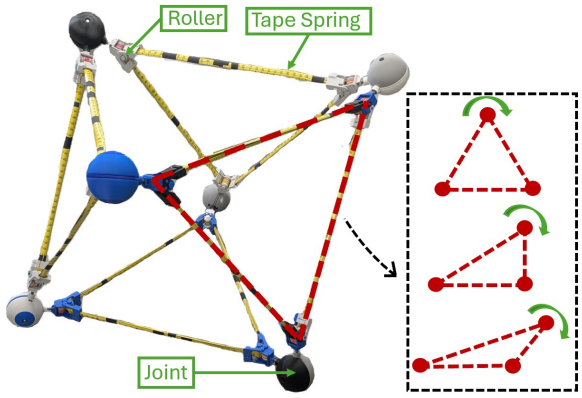

Fig. 1. Tape spring robot with major components labeled. The red dashed line indicates a single tape spring with 3 roller at each corner and to the side is an example of how the robot can change shape if one roller is actuated.

The use of a compliant, non-inflated structural member enables a new type of behavior - moving the tape spring independently while keeping the rollers stationary in 3D space. In prior inflatable designs, such as [1], the need for a valve at one roller restricted actuation to two rollers per triangular unit. By contrast, our design with three independently actuated rollers per triangle requires a new optimization framework that distributes motion across all nodes. This provides improved reconfiguration speed, robustness to component failure, and mobility.

The isoperimetric robot has several potential applications. One possible use is a reconfigurable positioning platform, similar to a Stewart platform, where its ability to change configurations can enable motion control for instruments or payloads. Another potential application is as a deployable mobile space structure, capable of expanding from a compact, collapsed state into a large, functional form once deployed. Its inherently small, collapsible size makes it advantageous for transportation, whether for terrestrial uses or for space missions where volume space is limited.

This paper explores the kinematic advantages of full-node actuation of the isoperimetric robot from tape springs and discusses the design, functionality, and potential applications

Manuscript received June 20 2025; revised August 19 2025; Accepted October 20 2025.

This paper was recommended for publication by Editor M. Ani Hsieh upon evaluation of the Associate Editor and Reviewers' comments. This work was supported by the Utah NASA Space Grant Consortium (NASA Grant No. 80NSSC20M0103), the 2024 NASA BIG Idea Challenge.)

[1]Nathan Usevitch, Fisk Lundgreen and Jackson Hancey are with the Ira A. Fulton School of Engineering, Mechanical Engineering Department, Brigham Young University, Provo. nathan_usevitch@byu.edu

Digital Object Identifier (DOI): see top of this page.

of the robot. We also present the mechanical design of key components (roller mechanism, joint system, tape springs, and mechatronic system) and evaluate the robot's capabilities in reconfiguration and structural strength.

This paper makes the following contributions:

- The concept and design of an isoperimetric truss robot where the structural member is a compliant beam, as opposed to an inflated tube.
- Kinematics of an isoperimetric robot where each triangle has three active rollers, as opposed to two active rollers and a static roller in [1].
- Optimal control of the isoperimetric robot that allows it to reach a configuration in minimum time assuming fixed speeds of each roller.

II. Related Work

A. Truss Robots

Truss-like modular robots have been proposed for applications such as exploring planets [3], shoring up rubble [4], [5], or as a shape-changing display or device [6]–[8]. The modular nature of truss components has led to the development of modular truss robotic systems [9]–[13]. A challenge in designing a truss robot is ensuring that actuators can achieve a sufficient extension ratio to enable significant shape change, as well as allowing the structure to be resilient to external loads and impacts. One approach is found in the related family of tensegrity robots, where some of the members of the truss are compliant tension elements [14], [15]. Another approach is to use pneumatic actuators [11]. The isoperimetric architecture, first introduced in [1], allows a high extension ratio and natural compliance by replacing multiple edges of the truss with an inflated beam. The robot changes shape by moving its joints along the inflated beam, allowing large changes in each edge length, but introducing the constraint that the length of the total member remain constant. Inflatable isoperimetric robots have been explored for lunar applications due to their ability to stow into a small volume during launch and then reconfigure for different tasks [2]. The presence of the inflated beam is prone to leaking and temperature-dependent pressure fluctuations, which has led us to explore structural members that work in an isoperimetric robot without requiring inflation.

B. Compliant Beams

The isoperimetric robot requires a structural member that allows a roller to induce and move joints continuously along its length. This requires that a roller mechanism can induce a region of low bending stiffness, but that the structural member achieves high stiffness away from the roller joint. Past isoperimetric robots have achieved this result with inflated tubes, but this characteristic is also demonstrated with tape springs in [16], [17]. In [17], a roller moves along a tape spring to create a manipulator. In [16] a combination of two tape springs that can unspool and several joints that can move along the tapes create a hyperredundant manipulator. The moveable buckling point in the tape measure is also used to create swimming robots [18] and pneumatic actuators [19]. Others have optimized the strength of slit-tube members [20], [21]. Our work extends this past work in moving joints by enabling tape springs and rollers to operate in a 3D, isoperimetric robotic system.

III. Robot Model and Control

A. Robot Definition

In order to control the robot we must define the relationships between the roller positions in 3D space, the edges lengths, and the positions of the rollers along the compliant beams. We define the state of the robot based on the connectivity of the edges (an undirected graph), the position of the vertices (the embedding) and how the edges are divided into triangles (denoted as a directed graph through the edges). We denote the graph $\mathcal{G} = (\mathcal{V}, \mathcal{E})$ where $\mathcal{V}$ is the set of vertices or nodes and $\mathcal{E}$ is the set of edges. The embedding of the robot, or the positions of its nodes, is given by the vector $x \triangleq [\boldsymbol{p}_1^\intercal, p_2^\intercal, \cdots, p_n^\intercal]$, $p_i \in R^3$. From these definitions of the edges and the node positions, we can compute the vector of all of the edge lengths of the graph, which we denote L.

We denote the position of roller i along its tape spring as d_i, and the vector of all roller positions as $\vec{D}$. As the beam is continuous, the position d_i wraps back to zero after it exceeds the total length of the tape spring. A diagram of a representative triangle is shown in Fig. 2. The relationship between the position of the rollers along the compliant beam d_i and the edge lengths of each triangle, L is

$$\begin{bmatrix} L_1 \\ L_2 \\ L_3 \end{bmatrix} = \begin{bmatrix} -1 & 1 & 0 \\ 0 & -1 & 1 \\ 1 & 0 & -1 \end{bmatrix} \begin{bmatrix} d_1 \\ d_2 \\ d_3 \end{bmatrix} = B\vec{D}. \tag{1}$$

Note that the matrix B is the transpose of the incidence matrix of the graph where the directed edges form a cycle around the triangle. We differentiate this expression to obtain a relationship between the velocities of the rollers along the tubes and the rate of change of the edge lengths:

$$\dot{L} = B\dot{\vec{D}}. \tag{2}$$

In previous isoperimetric robots, one of the rollers would be attached to the caps of the inflated tube and would remain in a fixed position, while the other two rollers move along the tube. In our case, all three rollers may be capable of moving along the tube. The matrix B, is rank 2. The nullspace of this matrix is spanned by the vector $\vec{1}$, as $0 = B\vec{1}$. When dealing with velocities as in Equation (2) , this corresponds to driving all of the rollers together, causing the tube to move through the rollers, but the edges lengths to remain constant. When dealing with positions, we denote this potential shift of all of the rollers together with the constant d_{shift}, and rewrite Equation (1) as

$$L = B(\vec{D} + 1d_{shift}) \tag{3}$$

One key difference between this theoretical definition of the robot and the physical realization is the presence of

offsets between the centers of rotation at the spherical joints, and the beams formed by the tape springs. In an ideal truss where the joints are in line with the structural members, externally applied loads will result in axial loads on the members. The presence of the offset in our robots means that the structural members will experience bending moments. Practically this does reduce the robots strength, and yet this idealized kinematic model still captures the movement characteristics of the robot.

B. Kinematics

We now define the kinematics of the robot that relate how motions in the roller positions along the beam change both the edge lengths and the node positions in $\mathcal{R}^3$. Eq. 2 gives the relationship between velocity of rollers along the beam and the change in edge lengths. To relate the motion of the nodes to the change in edge lengths, we have

$$\dot{L} = R(x)\dot{x} \tag{4}$$

where $R(x)$ is the scaled rigidity matrix in [1]. In order to constrain the robot to its environment, we also have $C\dot{x} = 0$, where each row of C constrains one of the rigid body motions of the robot structure. We combine these relationships to form the Jacobian of the robot.

$$\dot{x} = \begin{bmatrix} R(x) \\ C \end{bmatrix}^{-1} B^T \dot{\vec{D}} = J_\theta(x)\dot{\vec{D}} \tag{5}$$

The matrix $[R(x)^T C^T]^T$ will be full rank and invertible as long as the graph is infinitesimally rigid. This gives us the Jacobian, $J_\theta(x)$ relating the motion of the rollers along the beam to the motion of the nodes in $\mathcal{R}^3$.

C. Optimization

While two rollers per triangle is sufficient to achieve any feasible triangle shape, equipping each triangle with three active rollers enables faster and smoother motions. In this section, we solve the path-planning problem to determine the optimal way to move between any two configurations as quickly as possible, assuming each roller has a fixed maximum speed.

The starting configuration is defined as a triangle where the lengths are given by L_i, and the positions of the rollers along the beam is given by D_0. A desired final configuration is given in terms of edge lengths L_f. The optimization is to find the set of roller positions along the beam, D_f, that minimizes the time required to reach the final configuration, and satisfies the edge length constraint. We assume that the rollers can move at a constant speed, which means the fastest path between two configurations is the one that minimizes the longest distance that an individual roller must travel. We define the optimization as follows:

$$\min_{D_f} \left(\max(|\vec{D}_f - \vec{D}_0|) \right) \tag{6}$$

subject to

$$BD_f = L_f \tag{7}$$

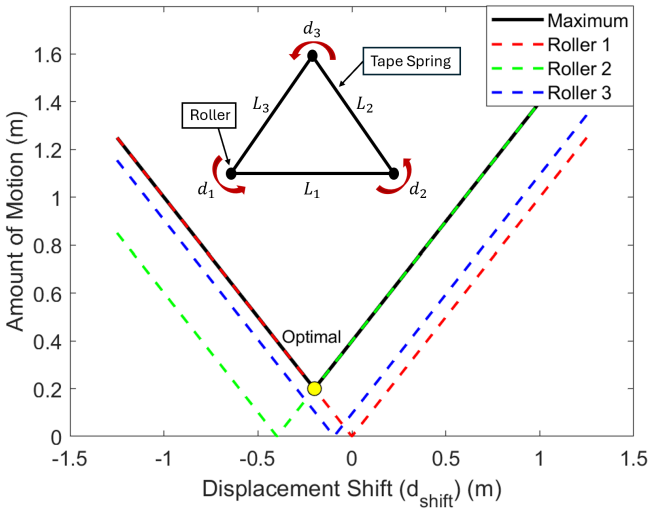

Fig. 2. Optimization of the shared displacement offset (d_{shift}) for a three-roller system in a specific configuration. The x-axis represents the common shift applied to all three rollers, while the y-axis shows the resulting absolute motion required by each roller. The solid black line indicates the maximum displacement among the three rollers for each d_{shift} value. The optimal value minimizes this maximum and is labeled and shown in yellow on the figure. Additionally, labeling for the robot definition of a single triangle is given above.

In a two-roller configuration, one roller distance will always be fixed, and there is a unique solution for the other two roller positions that gives a set of compatible edge lengths. In the three-roller configuration, there are an infinite number of roller positions that can give the same edge lengths. This remaining degree of freedom corresponds to the motion of moving all of the rollers together.

This is done by introducing a scalar shift d_{shift} to all rollers. This shift corresponds to driving all of the rollers together a uniform amount. We define $\vec{D_{f1}}$ as any valid solution constrained to Equation (7). In practice we define $\vec{D_{f1}}$ as the solution where roller 1 remains fixed at position 0.

$$\min_{d_{shift}} \left(\max(\left|\vec{D_{f1}} + \vec{1}d_{shift} - \vec{D}_0\right|) \right) \tag{8}$$

By running through a range of d_{shift} values we can find the optimal shift value that minimizes the longest motion as seen in Fig. 2. Solving this optimization in Equation (8) is equivalent to the optimization in Equation (6), but is over a single variable.

$$D^*_{final} = D_{f1} + \vec{1}d_{shift} \tag{9}$$

IV. Methods

A. Roller Design

The roller controls motion along the compliant beam, enabling reconfiguration of the robot's truss structure. To function effectively, it must grip the tape spring to prevent slippage, and pinch the tape to create a region of low bending stiffness that creates a joint. It must also preserve the rigidity of the beam away from the roller and withstand external forces from the joints housing the batteries and Printed

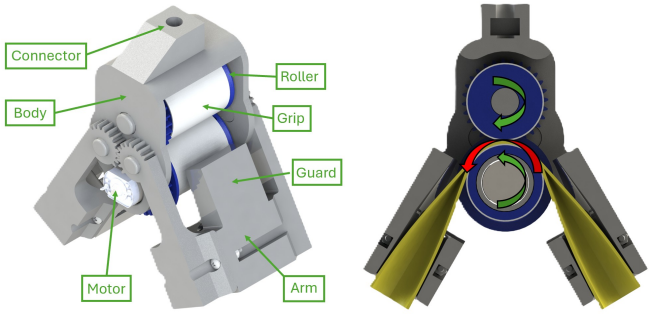

Fig. 3. (Left) Front view of roller with major components labeled. (Right) Sectional view of the roller with motion of the tape spring shown in red and motion of the rollers in green.

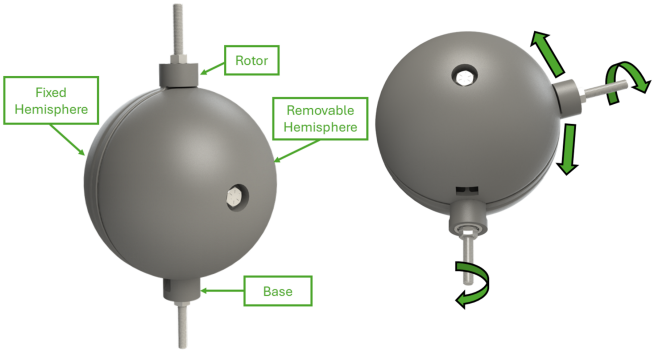

Fig. 4. The primary parts of the joint are shown. The electronics for the robot are housed inside (Left) and the 3 degrees of rotational freedom allow the robot to change shape without constraint from angle changes (Right)

Fig. 5. Assembly process of tape spring with (A) 12.5 cm tapered cut at each end, (B) taper ends are joined using spinnaker tape, and (C) final tape spring

Circuit Boards (PCBs). The roller assembly consists of 3D-printed PLA components for the arms, body, and rollers.

a) Rollers: The gripping mechanism uses dycem, non-slip material, wrapped twice around each roller to provide uniform grip on the tape spring. The grip strength is strong enough that when force is applied to the tape spring the motor reliably back drives as opposed to slipping relative to the roller. Closed loop control via the motor encoders enables accurate motion independent of variations in normal forces caused by the variations in the tape springs thickness as long as no slipping occurs. A DC motor [Pololu 3497] is housed in the bottom roller and is coupled via a metal hex adapter. Refer to Fig. 3 for the assembly of the roller.

b) Arms: The mechanical system uses two arms with varying cross sections to flatten the tape spring as it passes through the rollers, enabling proper bending. The top and bottom rollers are gear-linked, with a DC motor concentric to the bottom roller for compactness. An external gear system links the arms, ensuring the roller orientation bisects the angle formed by the tape spring. Refer to Fig. 3 for the mechanical movement of the roller.

B. Spherical Joint Design

The joint design connects two rollers together and uses 3 ball bearings to allow for all 3 rotational degrees of freedom to be unconstrained. The joint doubles as the housing for electronic control systems and can be opened for easy access to electronics without disconnecting the rollers. The joint is constructed from PLA plastic, 608z bearings, and 5/16-24 bolts. Each joint is made up of the parts shown in Fig. 4.

C. Tape Spring Design

The tape spring must support the structural loads of the robot in different configurations while moving smoothly through the rollers. A Milwaukee 40 ft tape measure was selected for its larger arc length of 35 mm, providing greater strength and stiffness than other commercial options. Additionally, it was readily available and cost effective, making it suitable for prototyping and testing.

For assembly, the tape was cut into 3 m lengths, with each end tapered about 12.5 cm, shown in Fig. 5, to enable smooth bending where the segments were joined. After cutting, the segments were joined together and an additional segment was attached back-to-back, forming a double-layer tape spring.

Segments were joined together using spinnaker tape, providing a secure yet flexible bond critical for roller motion. Because the lower tape spring has a shorter arc length than the upper, producing a slight slip between the layers at bends. The spinnaker tape accommodates this slip without tearing. Additional 2.5-5 cm segments of spinnaker tape were placed every 45 cm along the length of the tape spring, allowing for localized bending and increased freedom of motion around the joints while still preserving overall strength.

The double tape spring cross section consists of two mirrored circular arcs. Its structural properties depend on the roller-arm constraints. For example, a wider, thinner ellipse decreases bending stiffness, while a thicker ellipse (closer to a circle) increases stiffness.

The geometry of the double tape spring cross-section is shown in Fig. 6a. From this geometry we can define the following geometric relationships relating the width W, radius R, and arc angle θ:

$$sin(\theta) = \frac{W}{2R} \tag{10}$$

The arc length L_a is calculated by multiplying the circumference of a circle with a given radius R by the portion of the arc length included in the cross section. The arc length can then be multiplied by two to find the perimeter:

$$P = 4L_aR\pi\left(\frac{\theta}{2\pi}\right) \tag{11}$$

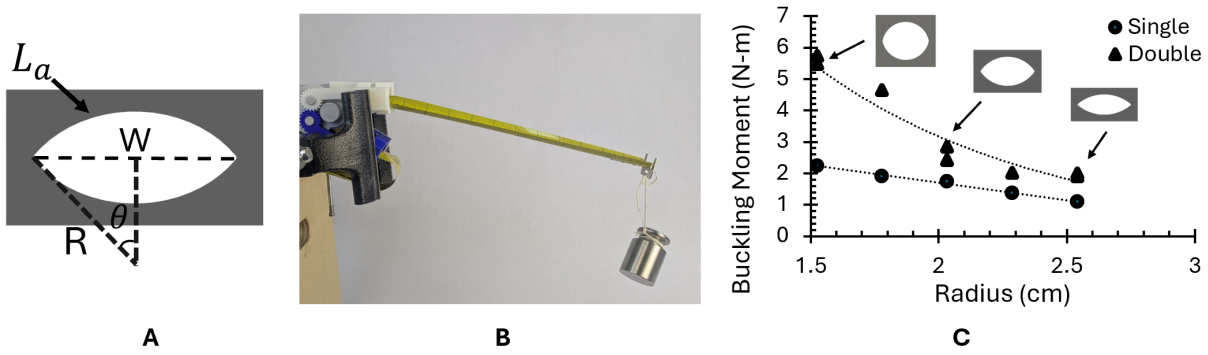

Fig. 6. (A) Cross section geometry of double tape spring with main dimensions labeled, (B) cross sectional test set-up for single tape spring, and (C) cross sectional test results for a single and double tape spring.

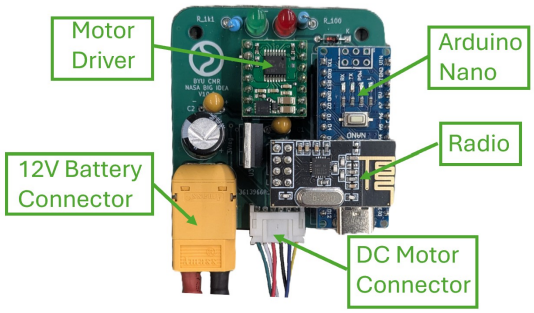

Fig. 7. Mechatronic System with major components labeled

Combining equations 10 and 11 we can solve for width:

$$W = 2R\sin\left(\frac{P}{2R}\right) \tag{12}$$

With this equation, we can manipulate the radius of the cross section and find the needed width to maintain a constant perimeter.

To evaluate the strengths of different cross sections, we tested tape springs with varying widths and radii using a cantilever setup as shown in Fig. 6b. The length of the cantilever beam was slowly extended until the tape spring buckled, and the failure moment was calculated from the mass and length. Tests with single and double tape springs under 500g and 1000g loads showed a negative correlation between radii and maximum moment. Additionally, we found that while smaller radii increase strength, they also hinder smooth movement through the roller's arms. Based on the results in Fig. 6c, we selected a 1.5 cm radii for the outer edge of the roller's arm, tapering to a 1.75 cm radii at the inner edge. This design achieves a balance between the strength of the tape spring while still allowing it to slide smoothly through the roller.

D. Mechatronic Design

The custom PCBs used were originally developed in [2]. The primary mechatronic difference between the two robots is that the tape spring robot has 12 rollers (3 per triangle) rather than 8 (2 per triangle), as in [2].

Mechanically, each roller has a corresponding PCB and each joint housed two PCBs and two 3-cell lithium polymer batteries. The electronics on the PCB are listed in Fig. 7. Communication between the PCBs is accomplished by 2.4 GHz radios on each PCB. With each PCB assigned with a unique identifier and commands coming from a master PCB.

V. Results

A. Component Testing - Single Triangle

a) Triangle Structural Test: We tested the strength of a single triangular unit by positioning the three nodes to form an equilateral triangle, fixing the two base nodes to prevent slippage and applying incremental weights to the top node until failure. The triangle supported 22.5 kg before collapsing and failure occurred by the tape spring bending between the main body of the roller and the arms, as shown in Fig. 8a. This suggests that the rollers, rather than the beams themselves, were the limiting factor in this configuration.

b) Comparing Multiple Rollers: We tested motion performance between two and three active rollers with a triangular component laid flat, with one node fixed in position (N1), another constrained to the x-axis (N2), and the final node free in 2D space (N3), as shown in Fig. 9.

Using the optimization procedure for the 2 and 3 roller configurations as described in the optimization section, we generated roller commands to move node 3 through four target positions, beginning at an initial equilateral triangle and moving counterclockwise before returning to its original position. The resulting trajectories, times, and distances traveled by node 3 were recorded for all 2 and 3 roller configurations. The average velocity was calculated by dividing the total distance by the total time. The results are summarized in Table. I.

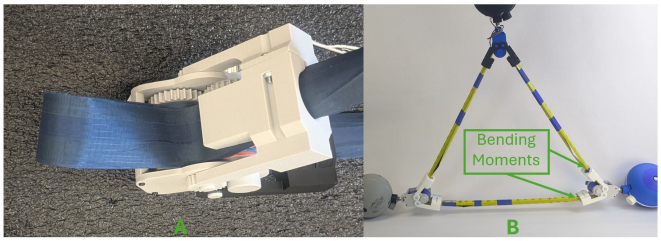

Fig. 8. Location of structural failure when placed under high load for single triangular unit (A) and full octahedron unit (B).

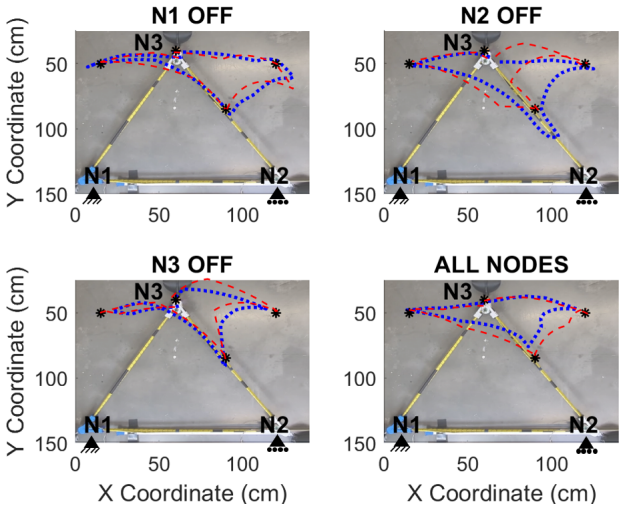

Fig. 9. X and Y axes are in centimeters. The tape spring triangle in the background indicates the initial starting location. The movement proceeds counterclockwise and returns to the original position. Node 1 is fixed in both x and y, Node 2 is fixed in y only, and Node 3 is free in both x and y. Black asterisks indicate the intended target positions, while the dotted blue line shows the actual path traced by Node 3 and the red dotted line shows the simulated optimal path.

From Fig. 9, each node configuration reached all four target points with minor error. The optimized paths (red) closely resemble the experimental ones (blue), especially in shape. Discrepancies between the two could stem from target misalignment, tape spring slippage, and roller speed variations. Table. I shows that the 3-roller configuration had the fastest velocity, showing evidence of its greater speed and optimized path compared to the 2-roller configuration.

B. Integrated System Testing - Octahedron

We performed a static load test on two octahedrons of different sizes as shown in Fig. 1 by applying force to one of the top joints until failure. Both the octahedron made of 3 m and 2.13 m structural members collapsed under a load of 4.5 kg. Both results are considerably lower than the 22.5 kg supported by a single triangle in the component test. This reduction of strength, and similar strength despite different scales, is likely due to bending moments introduced in the 3D structure at the roller arms, as shown in Fig 8b.

Similar to the single triangle motion test, we evaluated the efficiency of three active rollers per triangle compared to two active rollers and one fixed roller. We examined the motion of the octahedron where the top three nodes move upward in a piston-like fashion. This motion could be used in a repositioning platform in lifting or supporting objects. With all rollers active, the optimal motion is achieved by driving the top six rollers, regardless of the orientation of the octahedron. With only two active rollers per triangle, the same piston-like movement is possible, but it requires driving one of the rollers a greater distance. This case is illustrated in Fig. 10 between the 3 and 2 roller configurations.

Our results in Fig. 10 show the three-roller configuration reached the top in 4.66 seconds, while the two-roller configuration took 13.33 seconds. This was expected since, in the two roller case, two rollers had to move twice the distance as the other rollers. The three-roller configuration also enabled a symmetric, direct motion, while the two roller configuration caused the robot to follow an asymmetric, indirect path, as shown in the videos and in Fig. 10. Smoother motion could be achieved in the two roller case with incremental commands or varying roller velocities; however, the three roller configuration still allows faster and smoother transitions between distant configurations.

TABLE I
PERFORMANCE METRICS WITH DIFFERENT NODE CONFIGURATIONS

Node Config.	Time (s)	Total Distance (cm)	Average Velocity (cm/s)
N1 OFF	38.00	291.48	7.67
N2 OFF	37.33	299.60	8.03
N3 OFF	40.66	259.66	6.39
All Nodes	24.00	235.52	9.81

C. Locomotion

A key functionality of the isoperimetric robot is its ability to locomote by ”rolling” over one of its nodes. For the robot to move continuously, it requires two distinct rolling motions: rolling from a closed face (a single triangular unit flat on the ground) to an open face (a ground triangle formed by three triangular units), and vice versa. Fig. 11 depicts the robot transitioning from a closed face to an open face, with the first image illustrating the closed face state and the last showing the open face state. Similar to the piston motion, the three roller configuration provides the most efficient and stable rolling movement. However, during the transition from an open face to a closed face, the tape springs experienced buckling at the locations shown in Fig. 8. Additional movements from the robot can be seen in the attached video.

D. Deployment and Stowability

A key advantage of the tape springs is their ability to collapse into a more compact form, facilitating easier storage and transport. This feature is also present in the isoperimetric robot, making both designs well-suited for space travel [1]. As shown in Fig. 12, the isoperimetric robot from tape springs transitions from a fully deployed state to a fully collapsed state.

In its deployed configuration, the robot made from 3 m segments had an interior volume of approximately 0.775m^3. When collapsed, the robot can be approximated as a cylinder with a volume of $0.042\ \text{m}^3$. The robot made from 2.13 m segments had a volume of 0.317m^3 and a collapsed volume 0.032m^3. This results in a volume reduction factor of about 18.5 for the larger octahedron and 9.8 for the smaller.

VI. DISCUSSION

This work introduces an isoperimetric robot made from tape springs that departs from the inflatable tubes used in past isoperimetric robots. We will discuss the resultant increased actuation capability and robustness of the system, as well as the potential decrease in structural strength caused by this change.

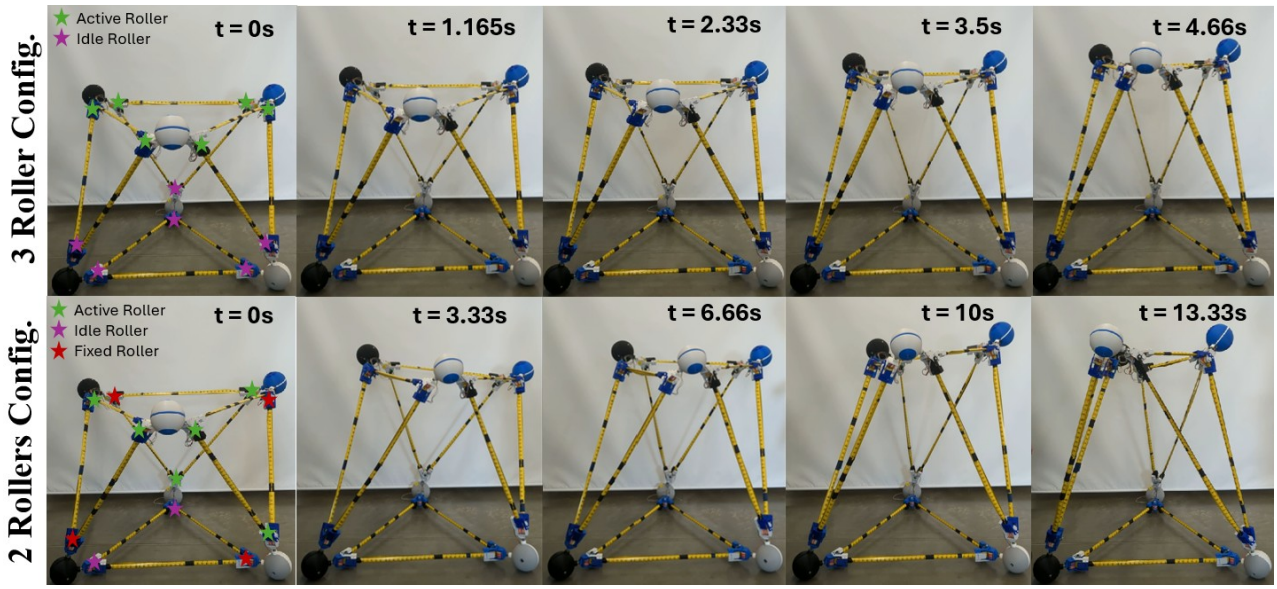

Fig. 10. Motion testing for 3 roller configuration (Top) and 2 roller configuration (Bottom) in full octahedron with time stamps for each frame indicated. The green stars indicate the active rollers, purple stars indicate idle rollers and the red stars indicate fixed rollers.

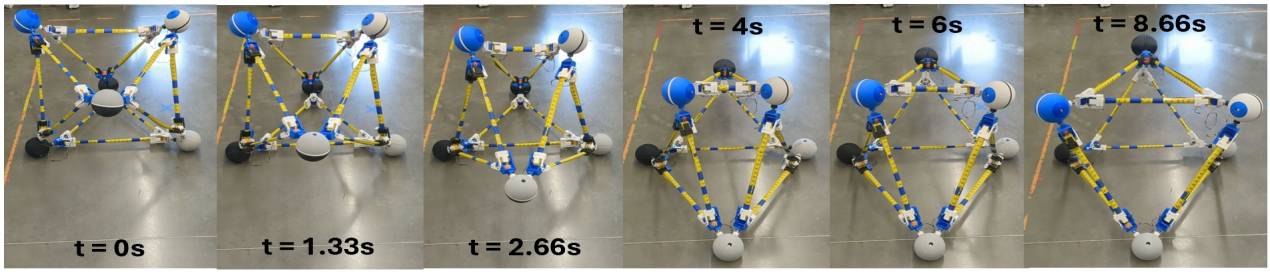

Fig. 11. Locomotion of the octahedron robot achieved by rolling over the top front node. Snapshots are shown with time stamps displayed above or below each frame. This demonstration uses the smaller octahedron robot.

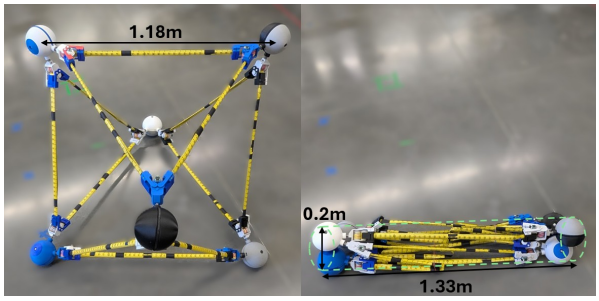

Fig. 12. Deployed vs fully collapsed robot for the robot made from 3 m segments

A. Actuation of all Rollers

One of the primary advantages of the tape spring beam-based robot is its ability to actuate all three rollers in each triangular module. This full-node actuation enables faster reconfiguration, more balanced and efficient motion paths, and improved overall robustness. In both component-level and full octahedron testing, the three-roller configuration consistently demonstrated the shortest path and fastest time to reach a target location. It also exhibited greater stability during piston tests. In contrast, the two-roller configuration caused the structure to sway during movement, reducing precision and control. The added speed and stability provided by full-node actuation give users greater control over the robot's movements and operational workspace.

Furthermore, the three-roller setup adds a layer of robustness. If one roller fails, the remaining two can continue to function, allowing the robot to remain mobile and functional.

B. Increased Robustness

Our tape spring beam-based isoperimetric robot successfully eliminated issues related to air leaks and temperature sensitivity [1], [2] by replacing the soft inflatable tubes with solid, tape springs. However, this approach introduced its own set of challenges.

One key issue was the inconsistent and often weak grip strength between the rollers and the tape spring. In the inflatable design, internal air pressure was pushed outward against the rollers, naturally maintaining a strong and uniform grip at each joint. In contrast, the grip strength of the tape spring, depended entirely on the force applied to pinch the beam between the rollers. To enhance this grip a non-slip material, dycem, was wrapped around the rollers, which did improve traction but still resulted in slight slipping at

the nodes under high external loads. Additionally, uneven roller grip sometimes caused motors to rotate at different speeds. Conversely, overly tight grip could hinder motor rotation entirely. One way to address this would be to include orientation sensors at each roller to help address drift over time due to small slipping events.

C. Structural Strength

The reduced strength observed in the full octahedron structure is largely due to the increased bending and torsional moments acting at the end of the roller's arms as seen in Fig. 8b. These moments diminish the overall structural integrity of the system. Therefore, improving the design to reduce the offset between the rollers and the joints would reduce the bending moments acting on the compliant beam and bring the structure closer to an ideal truss with more axial loads. Additionally, replacing the tape spring with stronger, more suitable compliant materials would further improve performance.

VII. Conclusion

In conclusion, the isoperimetric robot built with tape springs successfully addressed several challenges associated with soft inflatable tube-based designs. In particular, it eliminated issues such as air leaks and temperature-dependent performance, key issues that would prevent the isoperimetric robot from serving as a modular robotic structure for space applications. The use of tape springs also enables new behaviors, such as using motorized rollers at all vertices of the triangle to move the tape spring independently of the rollers position in 3D space. We have also presented an optimization that leverages this new ability to find the control inputs that allow the robot to transition between two known configurations in minimum time. However, the tape springs approach also introduced its own unique challenges, particularly related to structural strength and actuation consistency.

Future work could enhance the structural strength of the robot by replacing the tape spring with stronger, more suitable beam members. This upgrade should be accompanied by reinforcement of the rollers and joints to fully increase load-bearing capacity. Additionally, developing a configuration planning optimization that accounts for the structural strengths of the octahedron would prevent the structure from reaching weak configurations thereby enhancing overall strength and improving mobility.

References

[1] N. S. Usevitch, Z. M. Hammond, M. Schwager, A. M. Okamura, E. W. Hawkes, and S. Follmer, "An untethered isoperimetric soft robot," *Science Robotics*, vol. 5, no. 40, p. eaaz0492, 2020.

[2] M. Stanciu, S. Stowell, I. Weaver, A. Rose, C. Paul, J. Wade, A. Cerven, A. O'Bryan, B. Bodily, L. Yang, and N. Usevitch, "Untethered isoperimetric robotic truss for lunar applications," *BYU Scholars Archive*, 2025.

[3] S. Curtis, M. Brandt, G. Bowers, G. Brown, C. Cheung, C. Cooperider, M. Desch, N. Desch, J. Dorband, and K. Gregory, "Tetrahedral robotics for space exploration," *IEEE Aerospace and Electronic Systems Magazine*, vol. 22, no. 6, pp. 22–30, 2007.

[4] A. Spinos and M. Yim, "Towards a variable topology truss for shoring," in *2017 14th International Conference on Ubiquitous Robots and Ambient Intelligence (URAI)*. IEEE, 2017, pp. 244–249.

[5] E. Park, J. Bae, S. Park, J. Kim, M. Yim, and T. Seo, "Reconfiguration solution of a variable topology truss: Design and experiment," *IEEE Robotics and Automation Letters*, vol. 5, no. 2, pp. 1939–1945, 2020.

[6] R. Kovacs, A. Ion, P. Lopes, T. Oesterreich, J. Filter, P. Otto, T. Arndt, N. Ring, M. Witte, A. Synytsia *et al.*, "Trussformer: 3d printing large kinetic structures," in *Proceedings of the 31st Annual ACM Symposium on User Interface Software and Technology*, 2018, pp. 113–125.

[7] J. Gu, Y. Lin, Q. Cui, X. Li, J. Li, L. Sun, C. Yao, F. Ying, G. Wang, and L. Yao, "Pneumesh: Pneumatic-driven truss-based shape changing system," in *Proceedings of the 2022 CHI Conference on Human Factors in Computing Systems*, ser. CHI '22. New York, NY, USA: Association for Computing Machinery, 2022. [Online]. Available: https://doi.org/10.1145/3491102.3502099

[8] Y. Wang, K. Wang, Z. Wang, and K. Perlin, "Robotecture: A modular shape-changing interface using actuated support beams," in *Proceedings of the Nineteenth International Conference on Tangible, Embedded, and Embodied Interaction*, ser. TEI '25. New York, NY, USA: Association for Computing Machinery, 2025. [Online]. Available: https://doi.org/10.1145/3689050.3704925

[9] G. J. Hamlin and A. C. Sanderson, "Tetrobot modular robotics: Prototype and experiments," *in Proc. IEEE/RSJ International Conference on Intelligent Robots and Systems*, pp. 390–395, 1996.

[10] ——, "Tetrobot: A modular approach to parallel robotics," *IEEE Robotics and Automation Magazine*, vol. 4, no. 1, pp. 42–50, 2002.

[11] J. C. Zagal, C. Armstrong, and S. Li, "Deformable octahedron burrowing robot," in *Artificial Life Conference Proceedings*. Citeseer, 2012, pp. 431–438.

[12] A. Lyder, R. F. M. Garcia, and K. Stoy, "Mechanical design of odin, an extendable heterogeneous deformable modular robot," in *2008 IEEE/RSJ International Conference on Intelligent Robots and Systems*. Ieee, 2008, pp. 883–888.

[13] P. M. Wyder, R. Bakhda, M. Zhao, Q. A. Booth, S. Kang, M. E. Modi, A. Song, J. Wu, P. Patel, R. T. Kasumi, D. Yi, N. N. Garg, S. Bhutoria, E. H. Tong, Y. Hu, O. Mustel, D. Kim, and H. Lipson, "Robot links: Towards self-assembling truss robots," in *2024 6th International Conference on Reconfigurable Mechanisms and Robots (ReMAR)*, 2024, pp. 525–531.

[14] D. S. Shah, J. W. Booth, R. L. Baines, K. Wang, M. Vespignani, K. Bekris, and R. Kramer-Bottiglio, "Tensegrity robotics," *Soft robotics*, vol. 9, no. 4, pp. 639–656, 2022.

[15] A. P. Sabelhaus, J. Bruce, K. Caluwaerts, P. Manovi, R. F. Firoozi, S. Dobi, A. M. Agogino, and V. SunSpiral, "System design and locomotion of superball, an untethered tensegrity robot," in *2015 IEEE international conference on robotics and automation (ICRA)*. IEEE, 2015, pp. 2867–2873.

[16] T. Ding, B. Li, H. Liu, Y. Peng, and Y. Yang, "Planar multi-closed-loop hyper-redundant manipulator using extendable tape springs: Design, modeling, and experiments," *IEEE Robotics and Automation Letters*, vol. 7, no. 3, pp. 6630–6637, 2022.

[17] Y. Yang, Y. Qin, Y. Tang, Y. Yang, Y. Peng, and H. Pu, "Deployable closed-loop tape-spring manipulators with mobile drive components on localized folds," *Mechanism and Machine Theory*, vol. 167, p. 104553, 2022. [Online]. Available: https://www.sciencedirect.com/science/article/pii/S0094114X21003001

[18] C. Sparks, N. Justus, R. Hatton, and N. Gravish, "Amoeba-inspired swimming through isoperimetric modulation of body shape," in *2022 IEEE/RSJ International Conference on Intelligent Robots and Systems (IROS)*. IEEE, 2022, pp. 2685–2692.

[19] C. Sparks, T. Jin, and N. Gravish, "Pressure control of rolling-seal tape spring actuators," in *2024 IEEE 7th International Conference on Soft Robotics (RoboSoft)*. IEEE, 2024, pp. 722–727.

[20] A. J. Cook and S. J. Walker, "Experimental research on tape spring supported space inflatable structures," *Acta Astronautica*, vol. 118, pp. 316–328, 2016. [Online]. Available: https://www.sciencedirect.com/science/article/pii/S0094576515003872

[21] D. Piovesan, M. Zaccariotto, C. Bettanini, M. Pertile, and S. Debei, "Design and validation of a carbon-fiber collapsible hinge for space applications: A deployable boom," *Journal of Mechanisms and Robotics*, vol. 8, no. 3, p. 031007, 03 2016. [Online]. Available: https://doi.org/10.1115/1.4032271